Accepted Manuscript

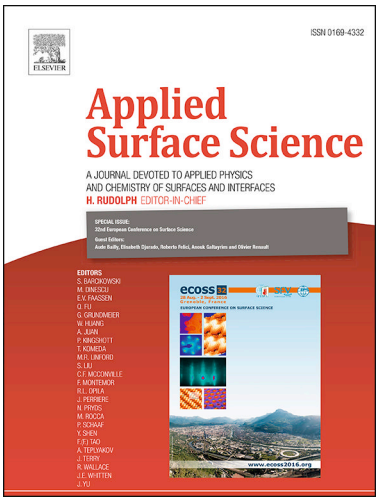

Full Length Article

Combustion synthesis of $Ce_2LuO_{5.5}$:Eu phosphor nanopowders: structure, surface and luminescence investigations

Shikao Shi, Dan Wei, Keyan Li, Shuping Wang, Lianshe Fu, Tao Yang, Lijian Meng

PII: S0169-4332(18)30730-X
DOI: https://doi.org/10.1016/j.apsusc.2018.03.060
Reference: APSUSC 38808

To appear in: *Applied Surface Science*

Received Date: 10 October 2017
Revised Date: 6 March 2018
Accepted Date: 8 March 2018

Please cite this article as: S. Shi, D. Wei, K. Li, S. Wang, L. Fu, T. Yang, L. Meng, Combustion synthesis of $Ce_2LuO_{5.5}$:Eu phosphor nanopowders: structure, surface and luminescence investigations, *Applied Surface Science* (2018), doi: https://doi.org/10.1016/j.apsusc.2018.03.060

Combustion synthesis of $Ce_2LuO_{5.5}$:Eu phosphor nanopowders: structure, surface and luminescence investigations

Shikao Shi [a,b,*], Dan Wei [a], Keyan Li [a], Shuping Wang [a], Lianshe Fu [b], Tao Yang [c], Lijian Meng [d]

[a] *College of Chemistry and Materials Science, Key Laboratory of Inorganic Nanomaterials of Hebei Province, Hebei Normal University, Shijiazhuang 050024, China*

[b] *CICECO, Department of Physics, University of Aveiro, 3810-193 Averio, Portugal*

[c] *Key Laboratoty of Biofuels, Qingdao Institute of Bioenergy and Bioprocess Technology, CAS, Qingdao 266101, China*

[d] *ISEP, Departamento de Fisica/Centre of Innovation in Engineering and Industrial Technology, Instituto Politecnico do Porto, Rua Dr. Antonio Bernardino de Almeida, 431, 4200-072 Porto, Portugal*

Abstract The spherical shape, uniform size and small degree of agglomeration of the particles play crucial roles in promoting the practical applications of the phosphor powders. In this paper, the novel Eu^{3+} -doped cerium lutetium $Ce_2LuO_{5.5}$ composite nanopowders with a cubic fluorite structure were prepared via a typical solution combustion route, and their internal structure, surface morphology as well as luminescence properties were investigated. The Eu^{3+} could substitute in either Lu^{3+} or Ce^{4+} sites and the existence of oxygen vacancy was confirmed in the composite by X-ray diffraction and Raman spectra techniques. Without the addition of surfactant, most of the as-prepared particles were bound together, and the luminescence was very weak even after a sintering process. Assisted with appropriate polyvinyl alcohol (PVA) surfactant in the combustion reaction and a subsequent heat-treatment process, the bound-particles were evidently separated and seemed to be nearly spherical shape. The particle size could be controlled to 30-120 nm and the luminescence was enhanced by adjusting the subsequent sintering temperature. Excited with 466 nm blue light, the nanopowders exhibited characteristic $^5D_0 \rightarrow {}^7F_J$ (J = 0~ 4) emission transition of Eu^{3+} and showed enhanced red luminescence as Eu^{3+} occupied Ce^{4+} site rather than Lu^{3+} site. The maximum emission was obtained as 40 mol% Eu substitutes Ce in the composite. Due to the coincidence of 466 nm excitation light with the

emission of InGaN chips in white light-emitting diodes, the surface-morphology improved Eu-doped $Ce_2LuO_{5.5}$ phosphor nanopowders have a potential application in solid state lighting fields.

Keywords Phosphor; Composite nanopowder; Combustion synthesis; Surfactant; Luminescence

*Corresponding author, Tel: +86-311-80787402, E-mail address: shishikao@hebtu.edu.cn

1. Introduction

Currently, the lanthanide ions-doped oxide phosphor powders are receiving substantial attention in the fields of lighting and display devices, optical communication, biological fluorescence labels as well as medical diagnostics due to their superior thermal stability, high luminescence efficiencies and tunable emission colors [1-4]. Generally, the oxide phosphor powders were traditionally prepared by a direct solid state reaction (SSR) process, in which the solid raw components were mixed, ground and then calcined at high temperature (1000~1500 ^{o}C) for a long duration. The preparation condition was not very difficult to reach. However, it suffered from a waste of energy and contamination of impurities, leading to inhomogeneous composition and morphology for the final samples. Therefore, the SSR process is not suitable to prepare the lanthanide ion –doped inorganic materials with controllable morphologies.

In contrast, a few soft chemical routes including hydro/solvothermal method, sol-gel process, spray pyrolysis and coprecipitation reaction have been used in the preparation of high quality lanthanide ion –doped phosphors with tunable morphologies and sizes (from nanometer to micrometer). These routes are based on solution-phase chemistry, in which the reactants can be homogenously mixed at molecular or ion level in solutions, resulting in the products to be precisely tuned in terms of size, shape and composition on the nanometer scale [5].

Among the lanthanide ion activators, the investigation of Eu^{3+}, Tb^{3+} and Eu^{2+} ions has been given more interests since they can emit characteristic red, green and blue

light when excited with ultra-violet (UV), cathode ray or X-rays, and can mix together to generate white light [6-9]. In particular, the Eu^{3+} -activated lanthanide oxide phosphors such as Y_2O_3: Eu with cubic structure has become a commercialized red phosphor in screen and fluorescent lighting since it can be efficiently excited with 254 nm UV and cathode rays [10]. To develop new oxide phosphor samples, the other types of lanthanide oxide such as CeO_2: Eu^{3+} and Lu_2O_3:Eu^{3+} were also studied by soft chemical routes in the past decade. For example, Jung et al. prepared CeO_2: Eu^{3+} nanopowders by a spray pyrolysis process, and noticed that the addition of certain Na^+ could obviously enhance the luminescence of Eu^{3+} [11]. Our group prepared CeO_2: Eu^{3+} nanoparticles by using solution combustion reaction and self-rising synthesis, and found that the Eu^{3+} -doped nanoceria showed characteristic red emission under the excitation of UV and X-ray [12,13]. On the other hand, Li's group synthesized mono-dispersed Lu_2O_3: Eu spheres by urea-based homogenous precipitation route, and densified into transparent ceramic after vacuum sintering. Upon UV excitation at 242 nm, the bright red emission line was detected for the powder and transparent ceramic [14]. However, the studies on the structure of CeO_2-Lu_2O_3 composite, surface morphology and luminescence of Eu^{3+} activated CeO_2-Lu_2O_3 composite, as far as we know, were seldom reported [15].

In this paper, the composite of CeO_2 and Lu_2O_3 (abbreviated as $Ce_2LuO5.5$) was prepared by a typical solution combustion synthesis (SCS), and Eu^{3+} ions were incorporated into the host. SCS is an effective reaction to prepare a variety of nanoscale oxides, which involves propagation of self-sustained exothermic reaction along an aqueous or sol-gel media [16]. Nevertheless, most crystallites of the as-prepared composite $Ce_2LuO_{5.5}$ had weak crystallinity and were not well separated due to the instantaneous reaction time (a few seconds) in the SCS process. Even after a post-sintering process, the surface morphology and luminescence of the samples were hardly improved.

It is known that the spherical shape, uniform size and small degree of agglomeration of the particles can effectively promote the practical applications of the phosphor powders in the optoelectronic devices [17]. To improve the surface

morphology and dispersity of the samples, the polyvinyl alcohol (PVA) surfactant molecules were added to the mixed solution in the combustion reaction. After the PVA –assisted combustion synthesis (PVACS) and a subsequent heat-treatment from 650~950 ^{o}C, the well-distributed composite particles with spherical shape and enhanced luminescence were achieved, which is quite beneficial for the potential applications.

2. Experimental procedure

In this work, the cerium lutetium composite $Ce_2LuO_{5.5}$ and Eu^{3+}-doped $Ce_2LuO_{5.5}$ crystalline powders were prepared by a simple SCS and PVACS. The raw materials include $Ce(NO_3)_3{\cdot}6H_2O$ (Yongda Chemical, Tianjin, 99.5%), Lu_2O_3 (Kangpeng Chem. Co. Ltd., Suzhou, 99.95%), Eu_2O_3 (General Institute of Non-ferrous Metals, Beijing, 99.95%), HNO_3(A.R.), urea(A.R.) and PVA(A.R.). At first, the $Lu(NO_3)_3$ and $Eu(NO_3)_3$ aqueous solutions were prepared by dissolving their respective oxides with dilute HNO_3. Then, the rare earth nitrate and urea were mixed in accordance with the molar ratio of Ce: Lu: Eu: urea = (2 : 1-x : x : 5) or (2-x : 1 : x : 5) to obtain a series of $Ce_2Lu_{1-x}O_{5.5}$: xEu^{3+} or $Ce_{2-x}LuO_{5.5-x/2}$: xEu^{3+} (x= 0.1~0.5) products. After the mixture was completely dissolved, the aqueous solution was put into a porcelain crucible to start a combustion reaction in a furnace, in which the temperature was kept at 550 ^{o}C. Soon, a bright flame was clearly observed from the top vent of the furnace and the combustion reaction lasted for only a few seconds. If the surfactant was not used in the process, the samples would occupy the entire space of the crucible with enormous swelling. To improve the surface shape and distribution of the particles, certain amount of PVA surfactant molecules (10~40 mol% in respect to the total amount of cations) were added to the mixed solution before the combustion reaction. After the PVACS, the as-prepared powders were well-spread in the bottom of the crucible without any swelling [18]. Then the samples were heat-treated at 650~950 ^{o}C for 2h. For the convenience of comparison, the $Ce_{1.733}Lu_{0.867}O_{5.37}$: $0.4Eu^{3+}$ in which Eu was assumed to uniformly distribute in cation sites, and $Ce_{0.86}O_{1.93}$: $0.14Eu^{3+}$ samples were also prepared by the above route.

The structure of the samples was studied with X-ray powder diffraction (XRD) patterns, which were measured with an X-ray diffractometer (BrukerD8 Advance) with CuKα (λ=1.5406Å) radiation at 40 kV and 40 mA. The Raman spectra of the samples were measured with a HORIBA JY HR800 confocal microscope Raman spectrometer using an Ar-ion laser (514.5 nm). The photoluminescence excitation and emission spectra were recorded using a spectrofluorometer (F-4600 Hitachi) equipped with a Xe lamp as the excitation source, and both excitation and emission slits were 2.5 nm. The photoluminescence decay curves and lifetime (τ) of the samples were taken by an Edinburgh FS5-TCSPC spectrofluorometer and the quantum efficiency (Q) values were calculated according to the lanthanide luminescence software package (LUMPAC) [19]. The surface morphology, particle size as well as the energy dispersive X-ray spectroscopy (EDS) of the powders were analyzed by a field emission scanning electron microscopy (SEM, S-4800 Hitachi). The particle size distribution data of the samples were collected through a Zetasizer Nano (ZS90, Malvern Panalytical). All the measurements were accomplished at ambient temperature.

3. Results and discussion

3.1 Structural analysis with XRD patterns and Raman spectra.

To investigate and confirm the structure of $Ce_2LuO_{5.5}$ composite nanoparticles prepared by SCS, the XRD patterns were measured. Fig. 1 gives the XRD patterns of $Ce_2LuO_{5.5}$ composite as well as the standard reference of CeO_2 and Lu_2O_3.The CeO_2 has the typical cubic fluorite structure corresponding to the *Fm3m* space group, and Lu_2O_3 has cubic crystal structure which belongs to *Ia3* space group. It can be seen that all the diffraction peaks for $Ce_2LuO_{5.5}$ are almost the same as that of CeO_2 (JCPDS no. 01-081-0792), and no other peaks ascribed to Lu_2O_3 (JCPDS no. 01-086-2475) are observed. Therefore, a new solid solution should be formed even without further heat-treatment. The peaks for $Ce_2LuO_{5.5}$ at 28.9°, 33.6°, 48.2°, 57.1°, 59.9°, 70.3°, 77.7° and 80.1°correspond to the (111), (200), (220), (311), (222), (400), (331) and

(420) planes, respectively, and most of the peak positions are quite close to those of the reference of pure CeO_2.The reason for this is that the effective ionic radius of Lu^{3+} (r = 1.12 Å) is almost equal to that of Ce^{4+} (r = 1.11 Å) in eight-fold coordination [20].

Fig. 2 and Fig. 3 show the XRD patterns of $Ce_2Lu_{1-x}O_{5.5}$: Eu^{3+} and $Ce_{2-x}LuO_{5.5-x/2}$: Eu^{3+} (x= 0 ~0.5) samples, respectively. The XRD peaks of all Eu–doped samples (Fig. 2a and Fig. 3a) are quite similar with that of $Ce_2LuO_{5.5}$, which indicate that the introduction of Eu^{3+} has little influence on the structure of the host. However, there is somewhat shift after Eu^{3+}doping to the composite due to the ionic radius difference of Eu^{3+} (r = 1.21Å) with Lu^{3+} and Ce^{4+}, and the shift can be clearly observed from Fig. 2b and Fig. 3b for the enlarged zone of (111) peaks of the XRD patterns. No matter which site Eu^{3+} locates, the peaks always shift towards lower 2θ angle direction due to the relatively larger Eu^{3+} ionic radius than that of Lu^{3+} and Ce^{4+}. Although the phenomena are different from what we have noticed in Eu –doped $Ce_2LaO_{5.5}$ [21], it is convinced that Eu^{3+} cations have entered into the host lattice and can occupy either Lu^{3+} or Ce^{4+} sites.

To further explore the variation of structure after Eu into Lu or Ce, the Raman spectra of $Ce_2LuO_{5.5}$, $Ce_2Lu_{0.6}O_{5.5}$: $0.4Eu^{3+}$, $Ce_{1.733}Lu_{0.867}O_{5.37}$: $0.4Eu^{3+}$ and $Ce_{1.6}LuO_{5.3}$: $0.4Eu^{3+}$ samples were measured and shown in Fig. 4. It is obvious that two Raman bands emerge in Fig. 4. The prominent one centered at about 460~ 465 cm^{-1} originates from the Raman-active F_{2g} mode corresponding to the oxygen breathing vibrations around Ce^{4+} [22], and the weak one centered around 560 ~570 cm^{-1} is due to the existence of certain amount of oxygen vacancies ($V_O^{"}$) [23]. In $Ce_2LuO_{5.5}$ and Eu^{3+} -doped $Ce_2LuO_{5.5}$ composites, Lu^{3+} and Eu^{3+} ions are incorporated to the cubic fluorite lattice. The substitution of Ce^{4+} with Lu^{3+} or Eu^{3+} will definitely result in the formation of $V_O^{"}$ defect owing to the different positive charge number and ion radius between Ce^{4+} with Lu^{3+} or Eu^{3+}.

The ratio of the peak area of the weak one to the prominent one (A_{570}/ A_{460}) is a good measure to estimate the number of $V_O^{"}$ in the composite [24], and has been listed in Table 1. The A_{570}/ A_{460} value is 0.4364 for pure $Ce_2LuO_{5.5}$ composite. With the introduction of Eu^{3+} into the composite, the A_{570}/ A_{460} value becomes large. When

Eu^{3+} ions replace Lu^{3+} rather than Ce^{4+} sites in $Ce_2Lu_{0.6}O_{5.5}$: $0.4Eu^{3+}$ sample, the A_{570}/ A_{460} value is increased to 0.5167. For $Ce_{1.733}Lu_{0.867}O_{5.37}$: $0.4Eu^{3+}$ sample in which Eu^{3+} ions are supposed to uniformly distribute in cation sites, the A_{570}/ A_{460} value is further increased to 0.5989. While for Eu^{3+} ions only occupy Ce^{4+} sites in $Ce_{1.6}LuO_{5.3}$: $0.4Eu^{3+}$ composite, the A_{570}/ A_{460} value is even increased to 0.6324. From the change of A_{570} /A_{460} value, it can be concluded that the unequal valence substitution of Ce^{4+} with Eu^{3+} can effectively facilitate the production of $V_O^{"}$ defect, and the equal valence substitution of Lu^{3+} with Eu^{3+} has not great effect on the number of $V_O^{"}$. With the increase of $V_O^{"}$ number, more serious distortion will occur in the host lattice. As a consequence, the luminescence properties of the composite system should be definitely influenced with the change of Eu^{3+} substitutive site.

The structure of the samples prepared by PVACS was also investigated. Fig. 5 shows the XRD patterns of the samples prepared by PVACS with and without further heat-treatment. All the diffraction peaks are consistent with the cubic fluorite structure of CeO_2 and $Ce_2LuO_{5.5}$. When the samples are achieved with the direct PVACS (without further heat-treatment), the diffraction peaks are relatively weak. After a subsequent sintering process, the diffraction peaks are evidently stronger than those by direct PVACS. With the increase of the sintering temperature from 650 to 950 ^oC, the diffraction peaks also gradually increase, manifesting that the post-heat-treatment process is favorable to improve the crystallization of samples.

3.2 Surface characteristics with EDS, SEM and particle size distribution analysis.

All the Eu –doped $Ce_2LuO_{5.5}$ powders mentioned in Fig. 2 and Fig. 3 were detected in the sample surface to achieve the molar ratio of metal elements Ce, Lu and Eu by EDS. The EDS technique is a semi-quantitative approach to detect the chemical element of the composition, and the detailed results are listed in Table 2. In spite of the existence of some deviations with the stoichiometric ratio, the data make us convince that the as-prepared samples are the designed products.

The typical surface morphologies of the phosphor samples were measured by SEM. Fig. 6 displays the SEM images prepared by simple SCS and PVACS assisted with

different amount of PVA (without further sintering). For the samples prepared by simple SCS (Fig. 6a), the estimated particle size is about 40-60 nm. Most crystallites are bound together and a few micropores can easily be observed. As the PVA is used with low concentration (10 mol%), the particle size looks smaller though the aggregation is not obviously improved (Fig. 6b). Assisted with suitable PVA concentration (20~30 mol%), most particles are well-separated and exhibit spherical shape (Fig. 6c and 6d). The particle size is mostly uniform and the average diameter of the particles is about 10 nm (Fig. 6c) and 30~50 nm (Fig. 6d), respectively. As the surfactant concentration reaches as high as 40 mol%, the serious aggregations with dense pores are formed (Fig. 6e). In consequence, the optimal surfactant concentration is determined to be 20 mol% in the combustion reaction.

To further analyze the effects of PVA surfactant on the composite powders, the particle size distribution of the samples was measured with Zetasizer Nano and shown in Fig. 6f. For the samples prepared with simple SCS, the medium particle size is around 273 nm, and the particle size ranges from 190 to 340 nm (black line in Fig. 6f). Assisted with suitable PVA surfactant, the particle size is evidently decreased and the particle size distribution gets narrow. For example, as the concentration of surfactant is 20 mol%, the medium particle size is 165 nm and the particle size ranges from 120 to 190 nm (green line in Fig. 6f). Since the particle size distribution data are collected from different means, the obvious deviations can be observed as compared to the data from SEM image. In spite of the existence of deviations, the results strongly manifest that the samples after the decoration with surfactant have relatively smaller particle size and more uniform particle distribution than those without the assistance of surfactants.

Additionally, the surface shape and particle size of the samples prepared with PVACS can be effectively controlled by adjusting the heat-treatment temperature. After a subsequent sintering process, most particles are well distributed and show clearly spherical or elliptical shape (Fig. 7a-d). The particle size is closely related to the heat-treatment temperature. With the increase of the sintering temperature from 650 to 950 ^{o}C, the particle size is gradually enlarged from 30 to 120 nm. The above

result implies that PVA surfactant can serve as an effective template to control the distribution of grains, and lead to the particles well-separated. The further sintering process promotes the grain growth and crystallization improvement, which is quite agreement with the XRD results in Fig. 5.

3.3 Luminescence studies with excitation and emission spectra.

Fig. 8 and Fig. 9 display the photoluminescence excitation and emission spectra of $Ce_2Lu_{0.6}O_{5.5}$: $0.4Eu^{3+}$, $Ce_{1.6}LuO_{5.3}$: $0.4Eu^{3+}$, and $Ce_{1.733}Lu_{0.867}O_{5.37}$: $0.4Eu^{3+}$, respectively. Moreover, the emission spectrum of $Ce_{0.86}O_{1.93}$: $0.14Eu^{3+}$ is also supplemented in Fig. 9 for the convenience of comparison. The purpose to choose the doping concentration of Eu^{3+} as 0.14 in Eu^{3+} -doped CeO_2 sample is to keep almost same content in respect to Eu^{3+}–doped composites as the total amount of cations is considered.

In the excitation spectra (Fig. 8) monitored with 612 nm, the weak band from 330 to 390 nm is ascribed to the O $\rightarrow$Ce charge transfer in the host [25], and the strong sharp lines at 393, 466 and 532 nm belong to the $^7F_0\rightarrow{}^5L_6$, $^7F_0\rightarrow{}^5D_2$ and $^7F_0\rightarrow{}^5D_1$ transitions of Eu^{3+}, respectively [26]. Among the excitation peaks, the dominant one is $^7F_0\rightarrow{}^5D_2$ transition at 466 nm. This means that the composite $Ce_2LuO_{5.5}$ can be well excited with blue light, which promotes its potential uses in white light-emitting-diodes owing to the coincidence with the emission of GaN chips [27]. In the following luminescent studies, the 466 nm at blue light region is selected as the efficient excitation wavelength.

Fig. 9 shows the emission spectra (λ_{ex}= 466 nm) of the above samples as well as $Ce_{0.86}O_{1.93}$: $0.14Eu^{3+}$. The emission spectra are very similar, and the peaks at 583, 593, (612, 630), 656 and 712 nm correspond to the characteristic $^5D_0\rightarrow{}^7F_J$ (J = 0, 1, 2, 3 and 4) transitions of Eu^{3+}, respectively [28]. Among the emission peaks, the predominant one is $^5D_0\rightarrow{}^7F_2$ electric dipole transition at 612 and 630 nm for all the samples, and therefore leads to the red light emission. Although these samples have similar emission peaks and same Eu doping content (as the total number of cations is considered), the evident emission intensities difference can be noticed. The

luminescence intensities of Eu^{3+}–doped composites are much higher than those of Eu^{3+}–doped CeO_2. In addition, the dramatic luminescence difference can be seen even for Eu^{3+}–doped $Ce_2LuO_{5.5}$ samples. If the relative emission intensity of $Ce_{0.86}O_{1.93}$: $0.14Eu^{3+}$ at 612 nm is 1, the relative emission intensity of $Ce_2Lu_{0.6}O_{5.5}$: $0.4Eu^{3+}$, $Ce_{1.733}Lu_{0.867}O_{5.37}$: $0.4Eu^{3+}$ and $Ce_{1.6}LuO_{5.3}$: $0.4Eu^{3+}$ is enhanced to 2.2, 3.5 and 5.1, respectively. It can be inferred from the result that Eu^{3+} substitution sites in the composite acts a crucial role in determining their luminescence intensities.

The Commission International de L'Eclairage (CIE) chromaticity coordinates of the related samples were also calculated using the emission spectra in Fig. 9, and the chromaticity coordinate values are listed in a Table 1. All of the CIE chromaticity coordinate values locate at red light region, and the chromaticity coordinate of $Ce_{1.6}LuO_{5.3}$:$0.4Eu^{3+}$ (0.604, 0.396) is more close to the standard value of pure red color (0.67, 0.33).

To achieve the optimal Eu doping concentration, the emission intensity dependence of $Ce_2Lu_{1-x}O_{5.5}$: xEu^{3+} and $Ce_{2-x}LuO_{5.5-x/2}$: xEu^{3+} (x= 0.1 ~0.5) on the Eu^{3+} doping concentration (x value) is shown in Fig. 10. At low concentration (x< 0.4), the emission intensity of Eu^{3+} for the two series of samples is gradually increased with the increasing Eu^{3+} doping concentration. As the Eu^{3+} doping concentration is more than 0.4, the emission intensity is obviously decreased. Therefore, the optimal Eu^{3+} doping concentration should be x= 0.4 in Eu^{3+}–doped composite $Ce_2LuO_{5.5}$. The reason for concentration quenching is that the distance between Eu^{3+} ions becomes shorter with the concentration increase of Eu^{3+}, and the collision or energy transfer from one luminescence center to another quenching center happens. Moreover, as can be seen from Fig. 10, the emission intensity of $Ce_{2-x}LuO_{5.5-x/2}$: xEu^{3+} is always superior to $Ce_2Lu_{1-x}O_{5.5}$: xEu^{3+} if the x value remains the same. This implies that the Eu^{3+} substitution for Ce^{4+} rather than Lu^{3+} site in $Ce_2LuO_{5.5}$ is advantageous to enhance the luminescence of the composite. Considering the Eu substitutive lattice and doping concentration, the optimal component of Eu- activated phosphor nanopowders is confirmed to be $Ce_{1.6}LuO_{5.3}$: $0.4Eu^{3+}$.

The photoluminescence emission of the samples prepared with PVACS and

subsequent heat-treatment are shown in Fig. 11. The luminescence intensity of the sample prepared by direct PVACS is the weakest due to its poor crystallization, as has been analyzed by XRD and SEM. After a subsequent sintering process, the emission intensity is gradually enhanced from 650 to 850 ^{o}C, and reaches maxima at 850 ^{o}C. As the sintering temperature is more than 850 ^{o}C (such as 950 ^{o}C), the emission intensity is decreased because of temperature quenching. Moreover, the optimized sample prepared by PVACS also exhibited enhanced luminescence as compared with that prepared by simple SCS. As can be seen from Fig. 9, the relative emission intensity for $Ce_{1.6}LuO_{5.3}$:0.4Eu^{3+} (the optimal component) is 5.1-fold in respect to $Ce_{0.86}O_{1.93}$: 0.14Eu^{3+} when prepared by simple SCS. While for the optimal component prepared by PVACS and a further sintering process, the relative emission intensity reaches 5.7, 7.2, 8.5 and 7.8-fold, which corresponds to the sintering temperature of 650, 750, 850, and 950 ^{o}C, respectively. Additionally, the luminescence decay curves for the samples corresponding to Fig. 11 were also measured and given in Fig. 12, and the fluorescent lifetime (τ) and quantum efficiency (Q) values of the samples were listed in Table 3. In Fig. 12, the luminescence decay for the sample prepared by direct PVACS is the fastest (τ = 0.534 ms) among all the samples and the Q value is 12.65%. After the subsequent heat-treatment process, the luminescence decay is prolonged and the Q value is increased gradually. As the heat-treatment temperature is 850 ^{o}C, the τ and Q values reach the maximum, which is 0.742 ms and 17.92%, respectively. Further increase the heat-treatment temperature to 950 ^{o}C leads to τ and Q values decrease. The above results imply that the PVACS method can not only improve the surface morphology and control particle size, but also enhance the luminescence intensity and quantum efficiency. The improved crystallization brings about a more even distribution of the activator Eu in the crystal lattice, and the larger particle size leads to a smaller number of non-radiation relaxation centers [29,30]. Therefore the luminescence intensity is gradually enhanced with the increase of the sintering temperature. This is a welcome change for the phosphor nanopowders potentially used in solid state lighting as well as other optoelectronic devices.

4. Conclusions

The Eu^{3+} -activated $Ce_2LuO_{5.5}$ composite phosphor nanopowders with a cubic fluorite structure were prepared by solution combustion reaction. After the Eu^{3+} is incorporated to the crystal lattice of $Ce_2LuO_{5.5}$ composite, it may occupy either Lu^{3+} or Ce^{4+} sites due to their close ionic radius. The $V_O^{"}$ in the host is generated owing to the difference of ionic radius and electric valence among Lu^{3+}, Ce^{4+} and Eu^{3+}. It has been confirmed from the Raman spectra that the number of $V_O^{"}$ in $Ce_{1.6}LuO_{5.3}$: $0.4Eu^{3+}$ is superior to that of $Ce_2Lu_{0.6}O_{5.5}$:$0.4Eu^{3+}$, which results in the difference of luminescent properties. Although all of the Eu^{3+} -activated composite samples can produce characteristic red-light emission of Eu^{3+} upon excitation at 466 nm, the composite system exhibits obviously enhanced luminescence as Eu^{3+} occupies Ce^{4+} site rather than Lu^{3+} site. The optimal component has been determined to be $Ce_{1.6}LuO_{5.3}$:$0.4Eu^{3+}$. Moreover, under the assistance with certain PVA surfactant in the combustion reaction process, not only the surface shape of the samples is effectively improved, but also the emission intensity and quantum efficiency are further enhanced. The Eu^{3+} -doped $Ce_2LuO_{5.5}$ phosphor nanopowders might be potentially applied in solid state lighting fields due to the coincidence of 466 nm excitation light with the emission of InGaN chips in white light-emitting diodes,

Acknowledgments

The authors would like to thank Dr. Ruilong Zong from Tsinghua University, who helped to measure the Raman spectra of the samples. This work was financially supported by Natural Science Foundation of Hebei Province (Grant No. E2015205159), China, Science Foundation of Hebei Education Department (Grant No.ZD2014045), China, High Level Talents Foundation in Hebei Province (Grant No.C201400327), China, and the Science Foundation of Hebei Normal University (Grant No. L2013K02), China.

References

[1] H.A. Höppe, Recent developments in the field of inorganic phosphors, Angew. Chem. Int. Ed. 48 (2009) 3572–3582.

[2] L. Chen, C.C. Lin, C.W. Yeh, R.S. Liu, Light converting inorganic phosphors for white light-emitting diodes, Materials 3 (2010) 2172–2195.

[3] C.Y. Liu, Y. Hou, M.Y. Gao, Are rare-earth nanoparticles suitable for in vivo applications? Adv. Mater. 26 (2014) 6922-6932.

[4] L.Y. He, Y.M. Su, L.H. Jiang, S.K. Shi, **Recent advances of cerium oxide nanoparticles in synthesis, luminescence and biomedical studies: a review, J. Rare Earths 33 (2015) 791-799.**

[5] S.L. Gai, C.X. Li, P.P. Yang, J. Lin, Recent progress in rare earth micro/nanocrystals: soft chemical synthesis, luminescent properties, and biomedical applications, Chem. Rev. 114 (2014) 2343-2389.

[6] Z.H. Leng, N.N. Zhang, Y.L. Liu, L.L. Li, S.C. Gan, Controlled synthesis of different multilayer architectures of $GdBO_3:Eu^{3+}$ phosphors and shape-dependent luminescence properties, Appl. Surf. Sci. 330 (2015) 270-279.

[7] L.E. Muresan, Y. Karabulut, A.I. Cadis, I. Perhaita, A. Canimoglu, J. G. Guinea, L.B. Tudoran, D. Silipas, M. Ayvacikli, N. Can, Tunable luminescence of broadband-excited and narrow line green emitting $Y_2SiO_5:Ce^{3+}$, Tb^{3+} phosphor, J. Alloy & Compd. 658 (2016) 356-366.

[8] W.G. Xiao, X. Zhang, Z.D. Hao, G.H. Pan, Y.S. Luo, L.G. Zhang, J.H. Zhang, Blue-emitting $K_2Al_2B_2O_7:Eu^{2+}$ phosphor with high thermal stability and high color purity for near-UV-pumped white light-emitting diodes, Inorg. Chem. 54 (2015) 3189-3195.

[9] X.G Zhang, M.Y. Chen, J.L. Zhang, X.Z. Qin, M.L. Gong, Photoluminescence studies of high-efficient red-emitting $K_2Y(WO_4)(PO_4):Eu^{3+}$ phosphor for NUV LED, Mater. Res. Bull. 73 (2016) 219–225.

[10] J.G. Li, X.D. Li, X.D. Sun, T. Ishigaki, Monodispersed colloidal spheres for uniform Y_2O_3:Eu^{3+} red-phosphor particles and greatly enhanced luminescence by simultaneous Gd^{3+} doping, J. Phys. Chem. C 112 (2008) 11707–11716.

[11] B.H. Min, J.C. Lee, K.Y. Jung, D.S. Kim, B.K. Choi, W.J. Kang, Aerosol synthesized CeO_2:Eu^{3+}/Na^+ red nanophosphor with enhanced photoluminescence, RSC Adv. 6 (2016) 81203-81210.

[12] S.K. Shi, M. Hossu, R. Hall, W. Chen, Solution combustion synthesis, photoluminescence and X-ray luminescence of Eu-doped nanoceria CeO_2:Eu, J. Mater. Chem. 22 (2012) 23461–23467.

[13] J.J. Wu, S.K. Shi, X.L. Wang, H.H. Song, M. Luo, W. Chen, Self-rising synthesis and luminescent properties of Eu^{3+} -doped nanoceria, J. Lumin. 152 (2014) 142–144.

[14] C. Ma, X.D. Li, S.H. Liu, Q. Zhu, D. Huo, J.G. Li, X.D. Sun, Fabrication of Lu_2O_3:Eu transparent ceramics using powder consisting of mono-dispersed spheres, Ceram. Inter. 41 (2015) 9577-9584.

[15] V. Grover, A. Banerji, P. Sengupta, A.K. Tyagi, Raman, XRD and microscopic investigations on CeO_2–am_2O_3 and CeO_2–an_2O_3 systems: a sub-solidus phase evolution study, J. Solid State Chem. 181 (2008) 1930-1935.

[16] A. Varma, A.S. Mukasyan, A.S. Rogachev, K.V. Manukyan, Solution combustion synthesis of nanoscale materials, Chem. Rev. 116 (2016) 14493-14586.

[17] N.O. Nuñez, S.R. Liviano, M. Ocaña, Citrate mediated synthesis of uniform monazite $LnPO_4$ (Ln = La, Ce) and Ln:$LaPO_4$ (Ln = Eu, Ce, Ce + Tb) spheres and their photoluminescence, J. Colloid Interf. Sci. 349 (2010) 484-491.

[18] J.J. Wu, S.K. Shi, X.L. Wang, J. B. Li, R.L. Zong, W. Chen, Controlled synthesis and optimum luminescence of Sm^{3+}-activated nano/submicroscale ceria particles by a facile approach, J. Mater. Chem. C 2 (2014) 2786-2792.

[19] J.D.L. Dutra, T.D. Bispo, R.O. Freire, LUMPAC lanthanide luminescence software: efficient and user friendly, J. Comput. Chem. 35 (2014) 772–775.

[20] The data of 8-coordinated ionic radii of Ce^{4+}, Lu^{3+} and Eu^{3+} are selected from the

website of www.webelements.com.

[21] S.K. Shi, K.Y. Li, S.P. Wang, R.L. Zong, G.L. Zhang, Structural characterization and enhanced luminescence of Eu-doped $2CeO_2$–$0.5La_2O_3$ composite phosphor powders by a facile solution combustion synthesis, J. Mater. Chem. C 5 (2017) 4302-4309.

[22] V.G. Keramidas, W.B. White, Raman spectra of oxides with the fluorite structure, J. Chem. Phys. 59 (1973) 1561-1562.

[23] Z.D. Dohcevic-Mitrovic, M.J Scepanovic, M.U. Grujic-Brojcin, Z.V. Popovic, S.B. Boskovic, B.M. Matovic, M.V. Zinkevich, F. Aldinger, The size and strain effects on the Raman spectra of $Ce_{1-x}Nd_xO_{2-\delta}$ ($0 \leq x \leq 0.25$) nanopowders, Solid State Commun. 137 (2006) 387-390.

[24] Z.Y. Pu, J.Q. Lu, M.F. Luo, Y.L. Xie, Study of oxygen vacancies in $Ce_{0.9}Pr_{0.1}O_{2-\delta}$ solid solution by in situ X-ray diffraction and in situ Raman spectroscopy, J. Phys. Chem. C 111 (2007) 18695-18702.

[25] G. Vinothkumar, R. Amalraj, K.S. Babu, Fuel-oxidizer ratio tuned luminescence properties of combustion synthesized Europium doped cerium oxide nanoparticles and its effect on antioxidant properties, Ceram. Inter. 43 (2017) 5457-5466.

[26] S.K. Shi, X.R. Liu, J.Gao, J. Zhou, Spectroscopic properties and intense red-light emission of (Ca, Eu, M)WO_4 (M = Mg, Zn, Li), Spectrochim. Acta. Part A 69 (2008) 396-399.

[27] Z.G. Xia, Q.L. Liu, Progress in discovery and structural design of color conversion phosphors for LEDs, Prog. Mater. Sci. 84 (2016) 59-117.

[28] S.K. Shi, J. Gao, J. Zhou, Effects of charge compensation on the luminescence behavior of Eu^{3+} activated $CaWO_4$ phosphor, Opt. Mater.30 (2008) 1616-1620.

[29] S. K. Shi, H. L. Gong, J. J. Wu, M. Luo, J. Zhou, Synthesis of Eu^{3+}-activated $La_2Mo_2O_9$ powder phosphors by surfactant-assisted hydrothermal approach, J. Am. Ceram. Soc. 95 (2012) 3878-3882.

[30] A.K.V. Raj, P.P. Rao, T.S. Sreena, V. James, U.A. Renju, Remarkable changes in the photoluminescent properties of $Y_2Ce_2O_7$:Eu^{3+} red phosphors through

modification of the cerium oxidation states and oxygen vacancy ordering, Phys. Chem. Chem. Phys. 16 (2014) 23699-23710.

Figure caption

Fig. 1. XRD patterns of $Ce_2LuO_{5.5}$ composite powder as well as the standard reference of CeO_2 and Lu_2O_3.

Fig. 2. XRD patterns of the $Ce_2Lu_{1-x}O_{5.5}$: xEu^{3+} (x=0~0.5) samples prepared by simple SCS: (a) wide-angle patterns and (b) enlarged-zone patterns for (111).

Fig. 3. XRD patterns of the $Ce_{2-x}LuO_{5.5-x/2}$: x Eu^{3+} (x=0~ 0.5) samples prepared by simple SCS: (a) wide-angle patterns and (b) enlarged-zone patterns for (111).

Fig. 4. Raman spectra of $Ce_2LuO_{5.5}$ and Eu^{3+} -doped $Ce_2LuO_{5.5}$ samples.

Fig. 5. XRD patterns of the $Ce_{1.6}LuO_{5.3}$:$0.4Eu^{3+}$ prepared by direct PVACS and a subsequent heat-treatment process from 650 to 950 ^oC.

Fig. 6. SEM images of $Ce_{1.6}LuO_{5.3}$:$0.4Eu^{3+}$ prepared by SCS assisted with different stoichiometric ratio of PVA (a) 0, (b) 0.1, (c), 0.2, (d) 0.3, (e) 0.4 and their particle size distribution analysis(f).

Fig. 7. SEM images of $Ce_{1.6}LuO_{5.3}$:$0.4Eu^{3+}$ prepared by PVACS and a subsequent heat-treatment at (a) 650^oC, (b) 750^oC, (c) 850 ^oC and (d) 950 ^oC.

Fig. 8. Excitation spectra of Eu^{3+} -activated $Ce_2LuO_{5.5}$ samples monitored with 612 nm.

Fig. 9. Emission spectra of Eu^{3+} -activated $Ce_2LuO_{5.5}$and CeO_2 samples excited with 466 nm blue light.

Fig. 10. The emission intensity dependence of $Ce_2Lu_{1-x}O_{5.5}$:xEu^{3+} and $Ce_{2-x}LuO_{5-x/2}$: xEu^{3+} (x= 0.1 ~0.5) on the Eu^{3+} doping concentration (x value).

Fig. 11. Emission spectra of optimized component $Ce_{1.6}LuO_{5.3}$:$0.4Eu^{3+}$ prepared by direct PVACS and a subsequent sintering process from 650 to 950^oC.

Fig. 12. The luminescence decay curves of optimized component $Ce_{1.6}LuO_{5.3}$:$0.4Eu^{3+}$ prepared by direct PVACS and a subsequent sintering process from 650 to 950^oC.

Figure 1

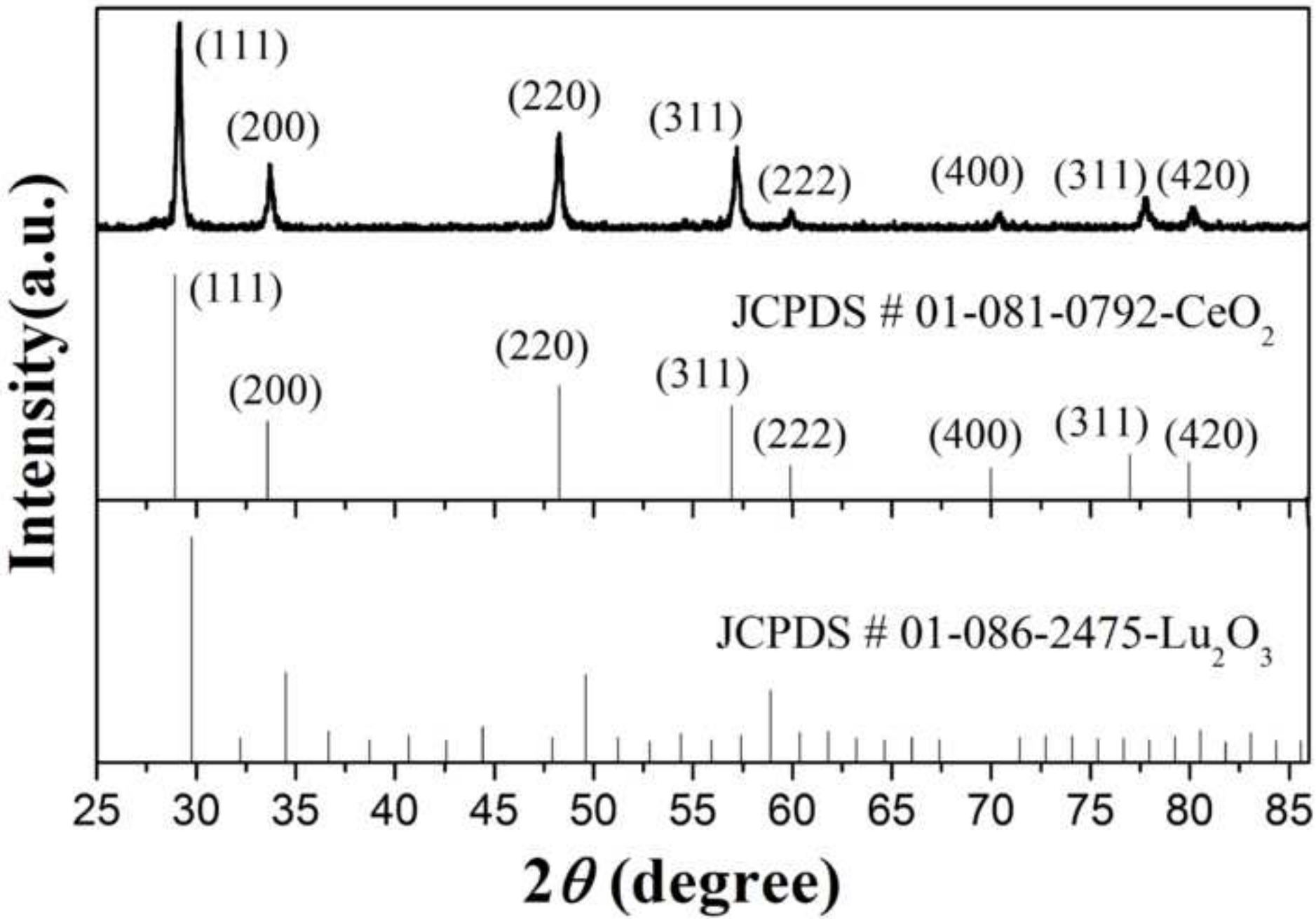

Figure 2

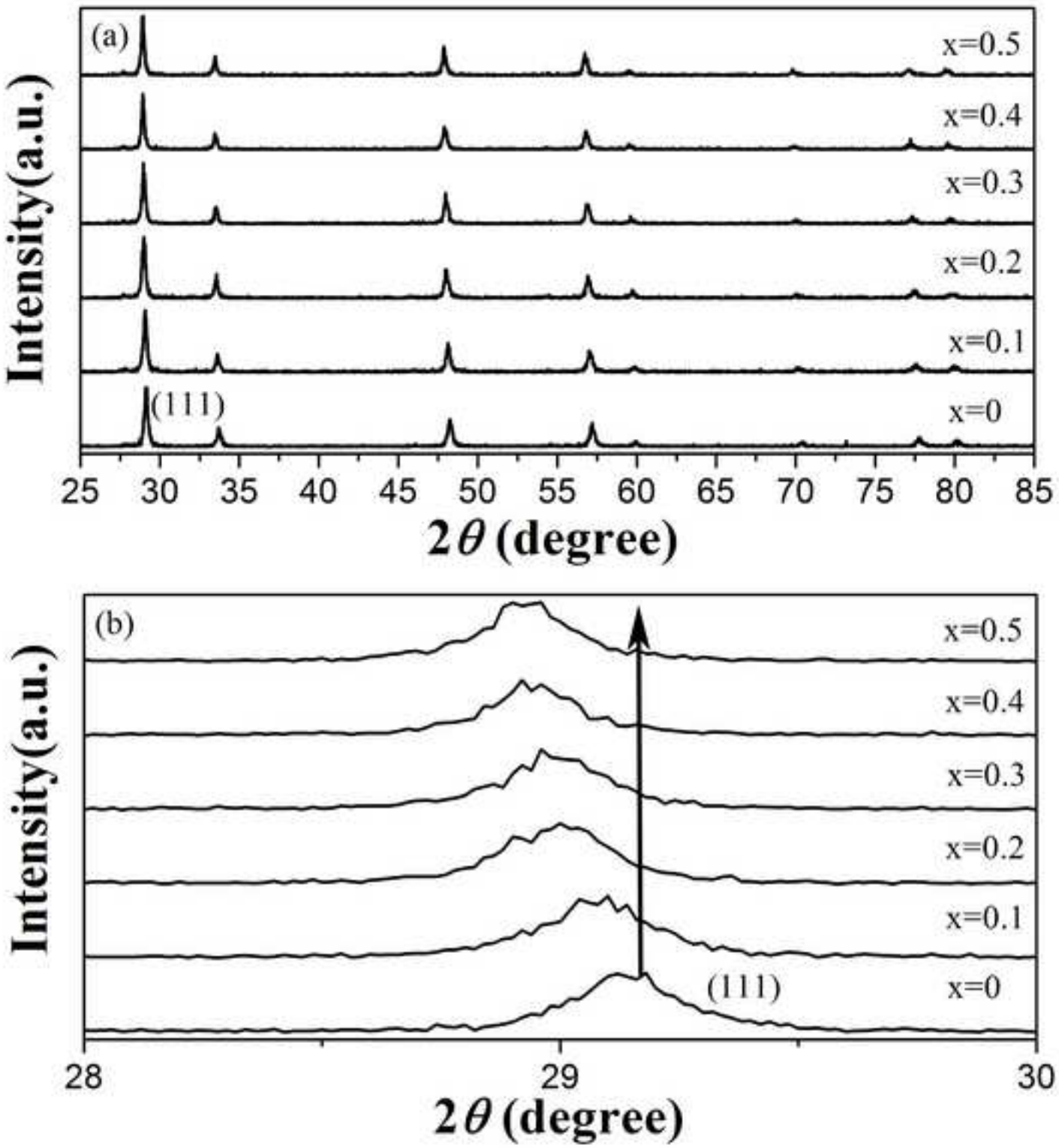

Figure 3

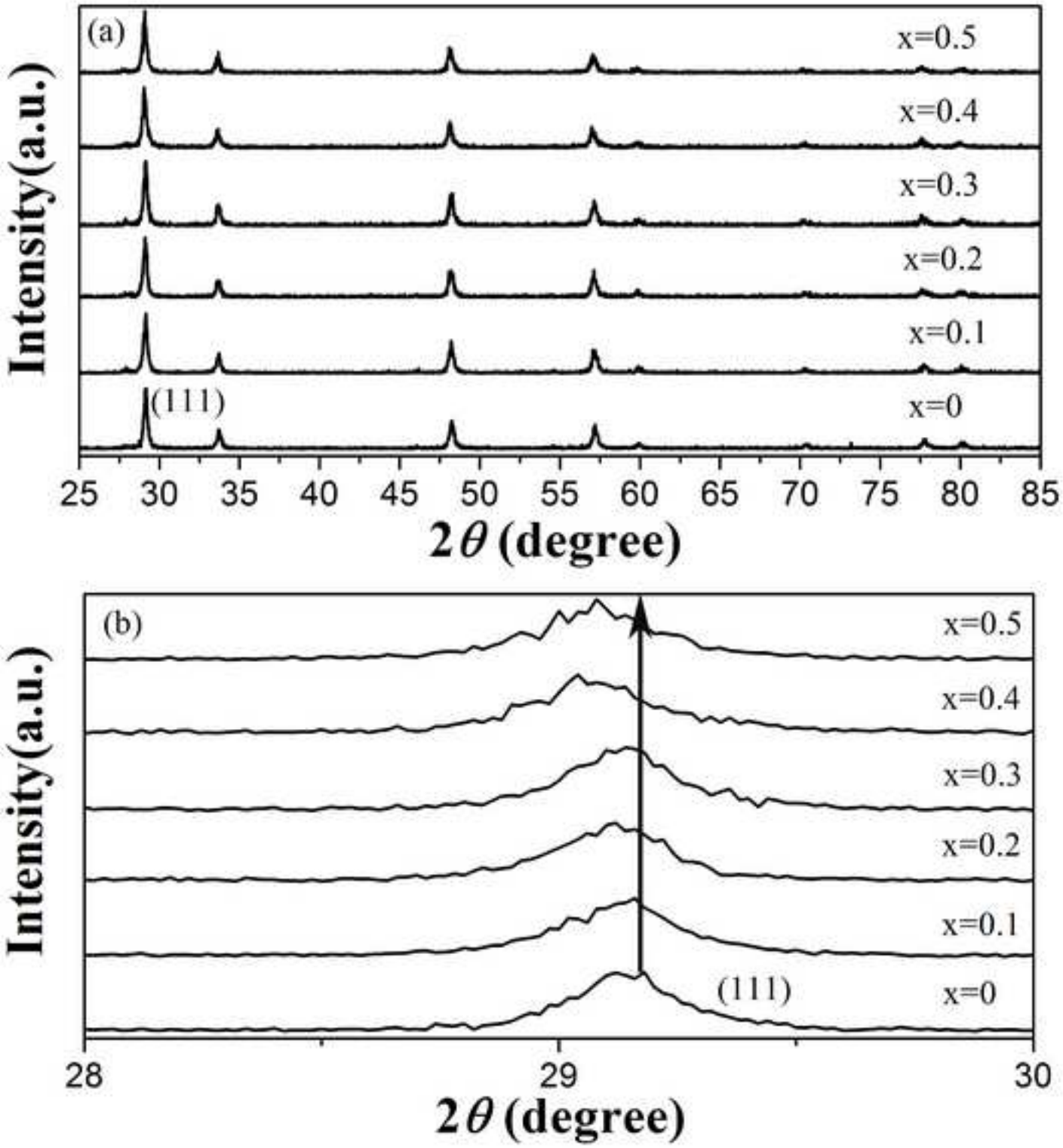

Figure 4

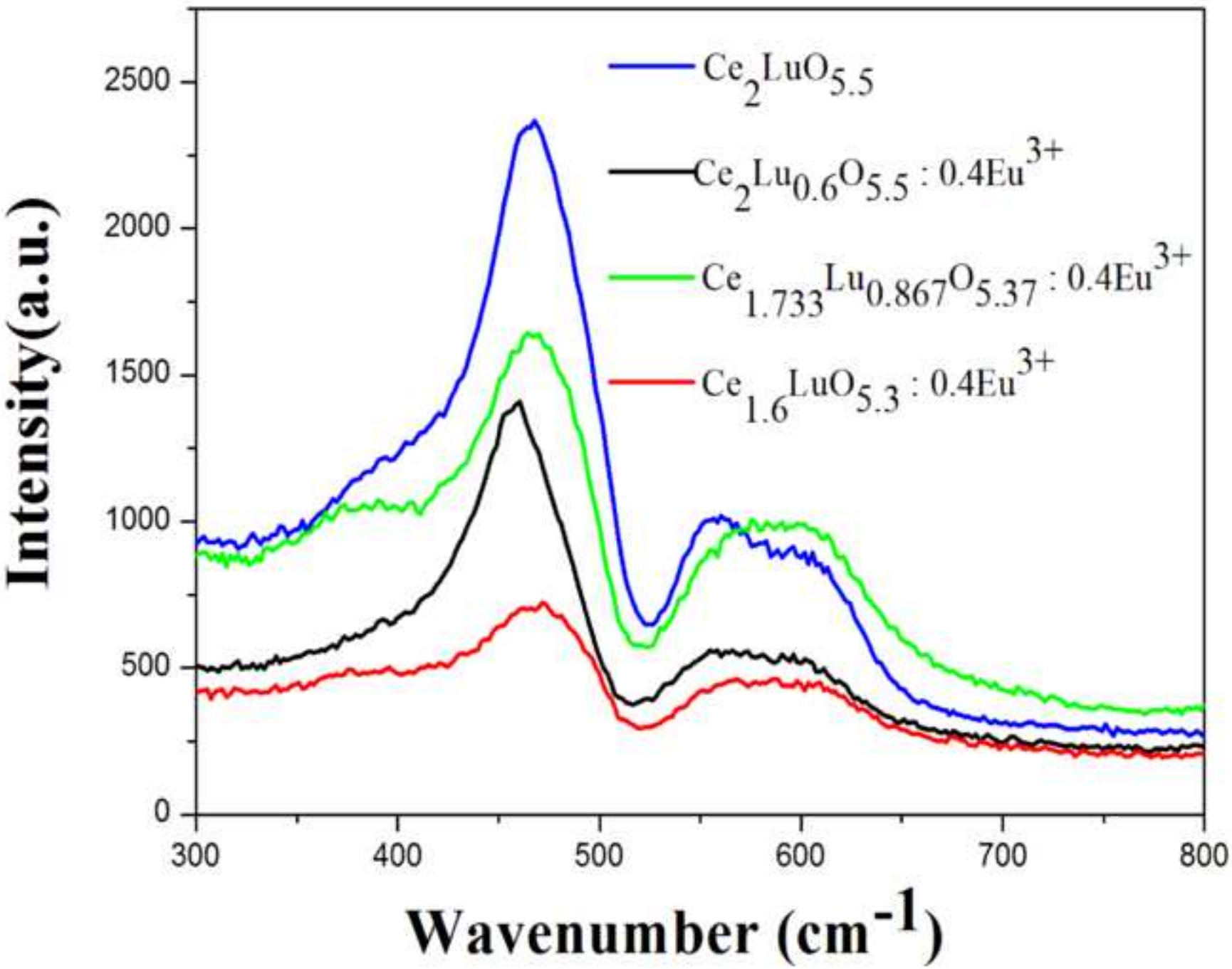

Figure 5

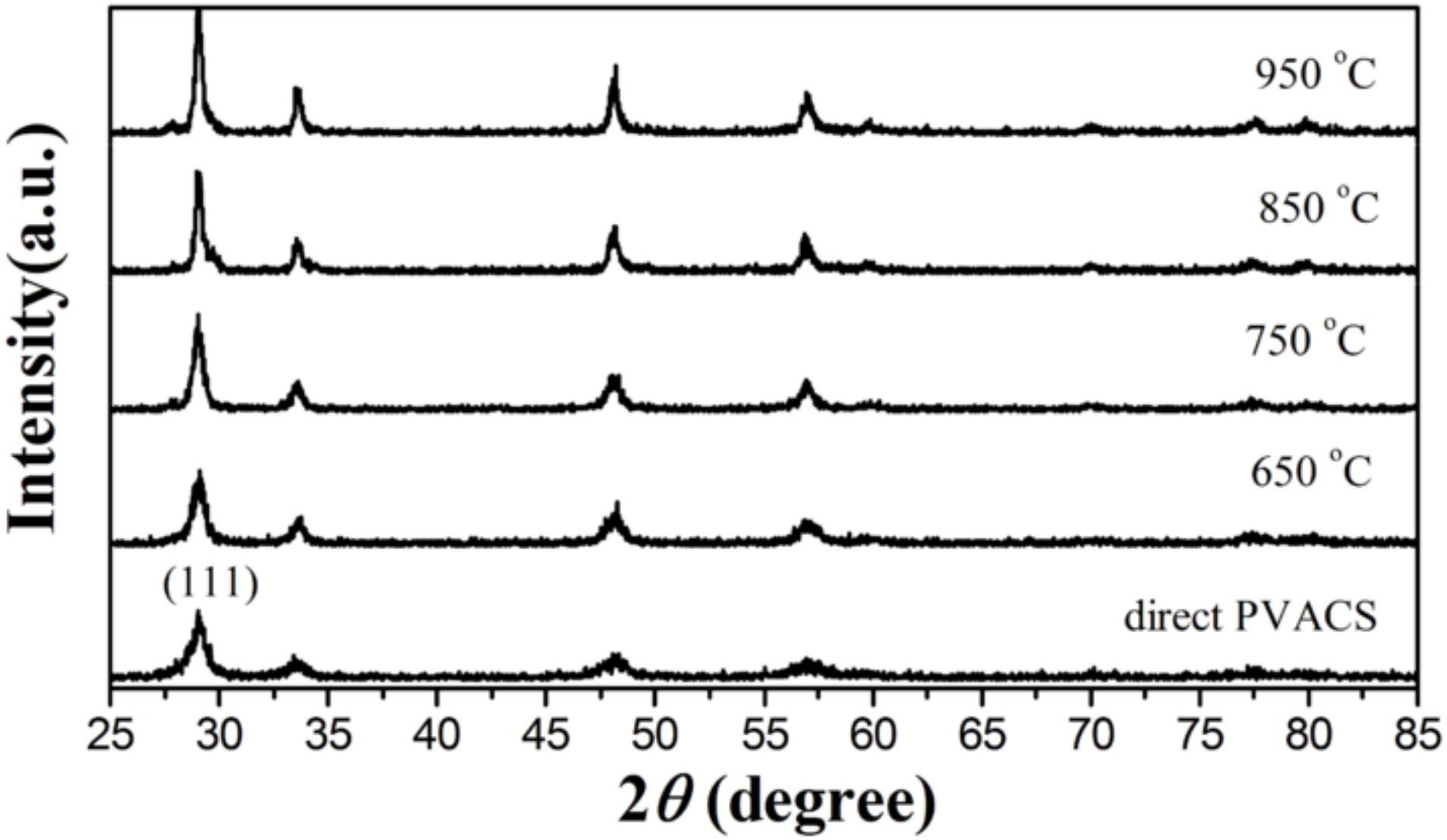

Figure 6

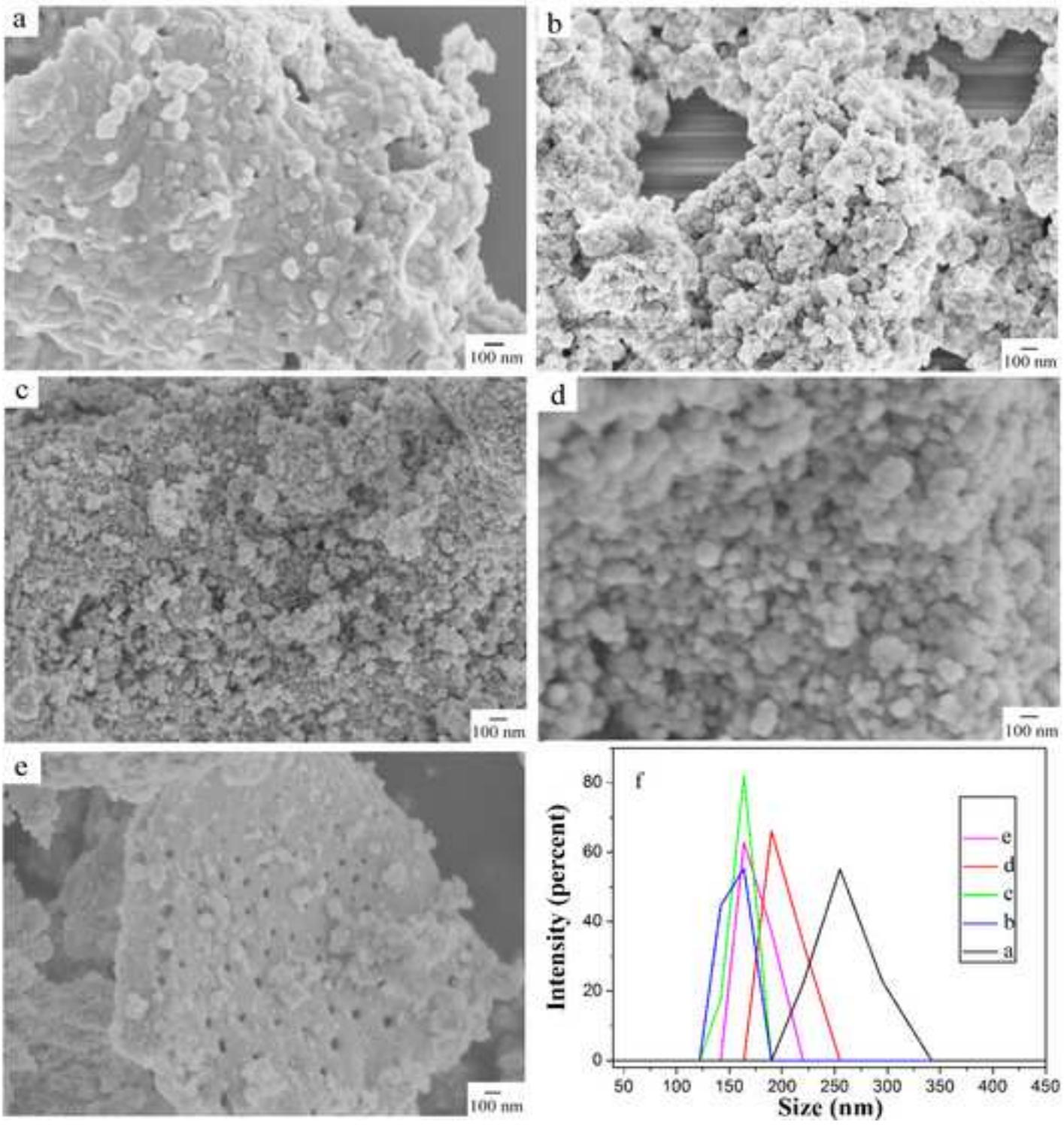

Figure 7

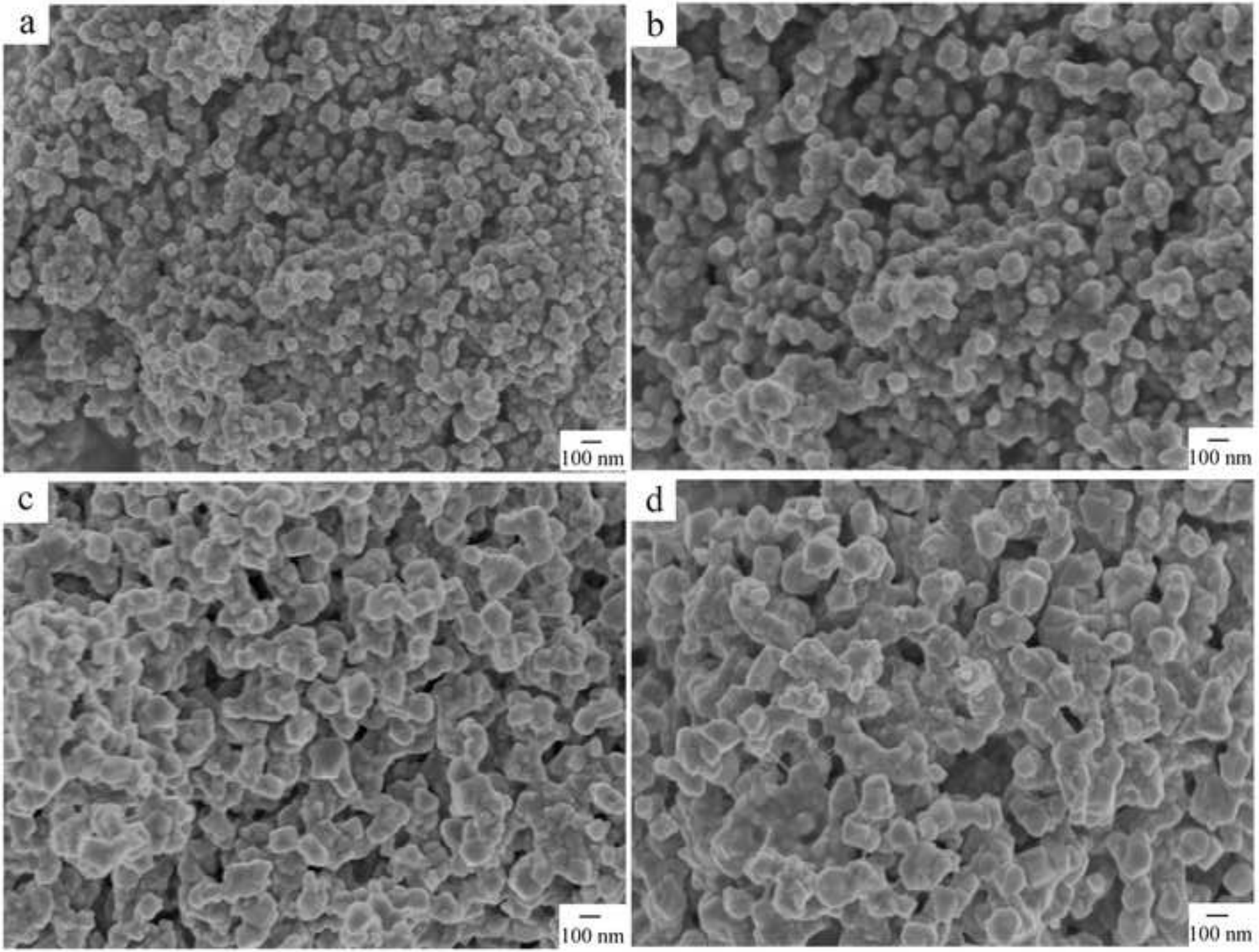

Figure 8

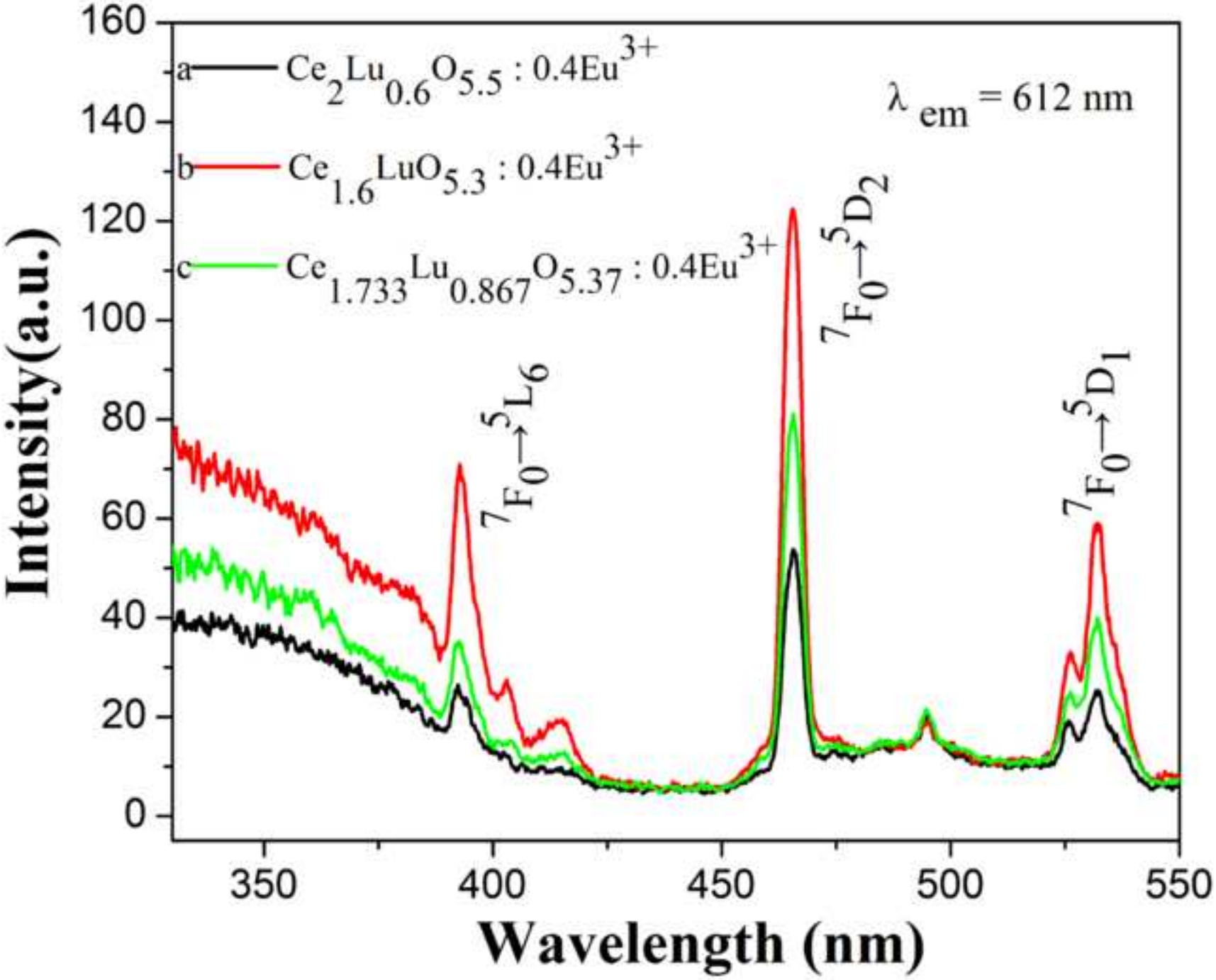

Figure 9

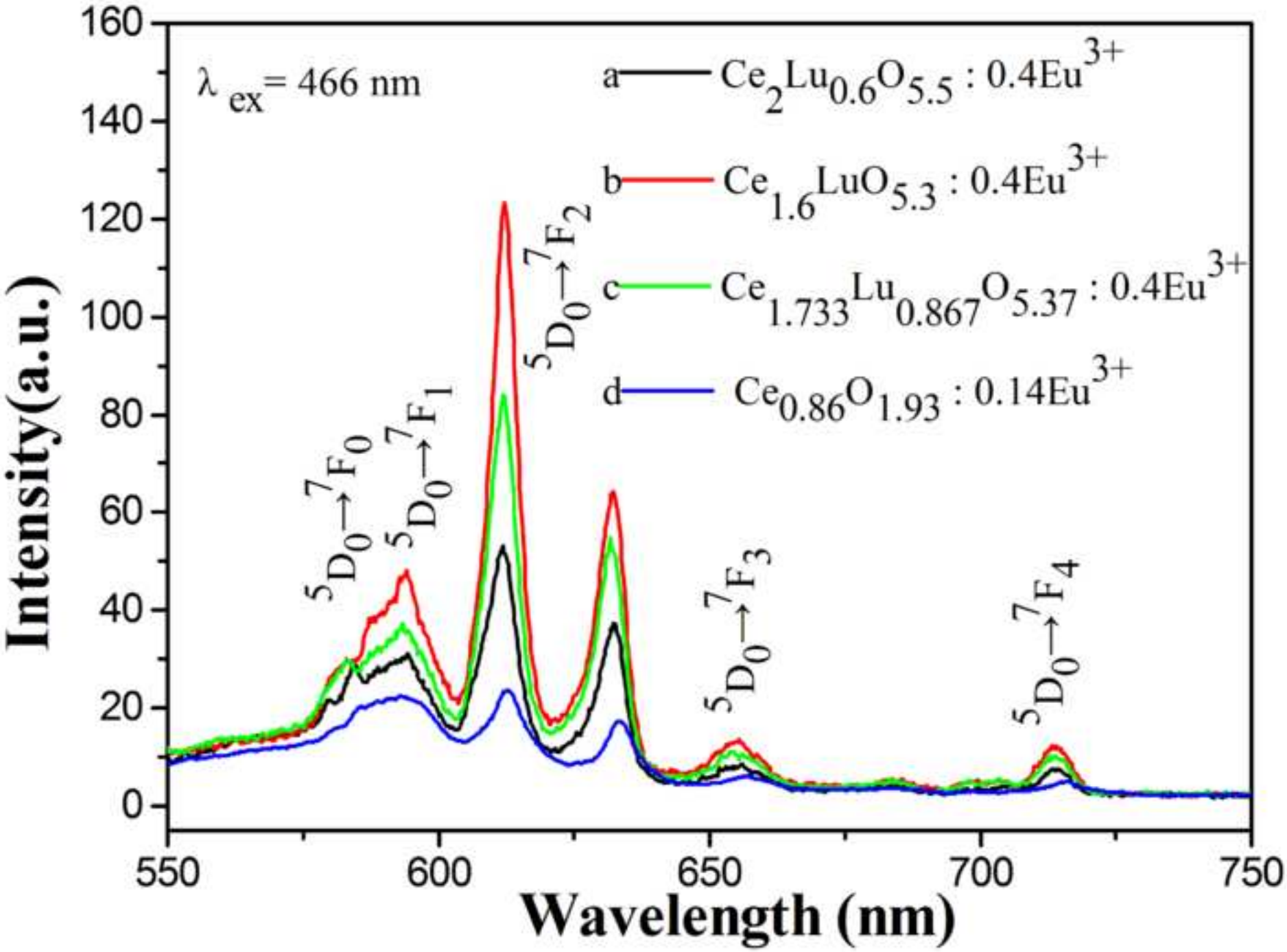

Figure 10

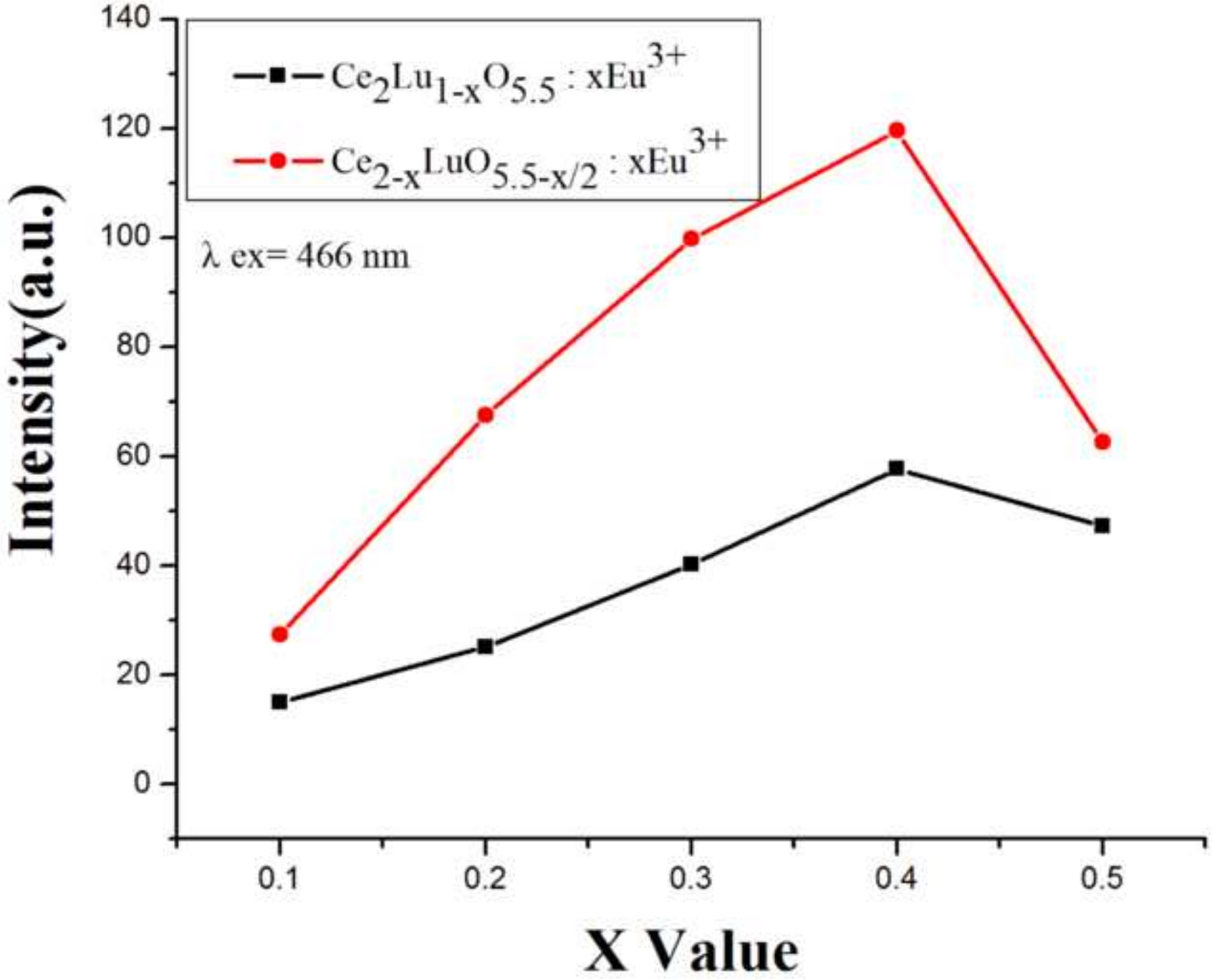

Figure 11

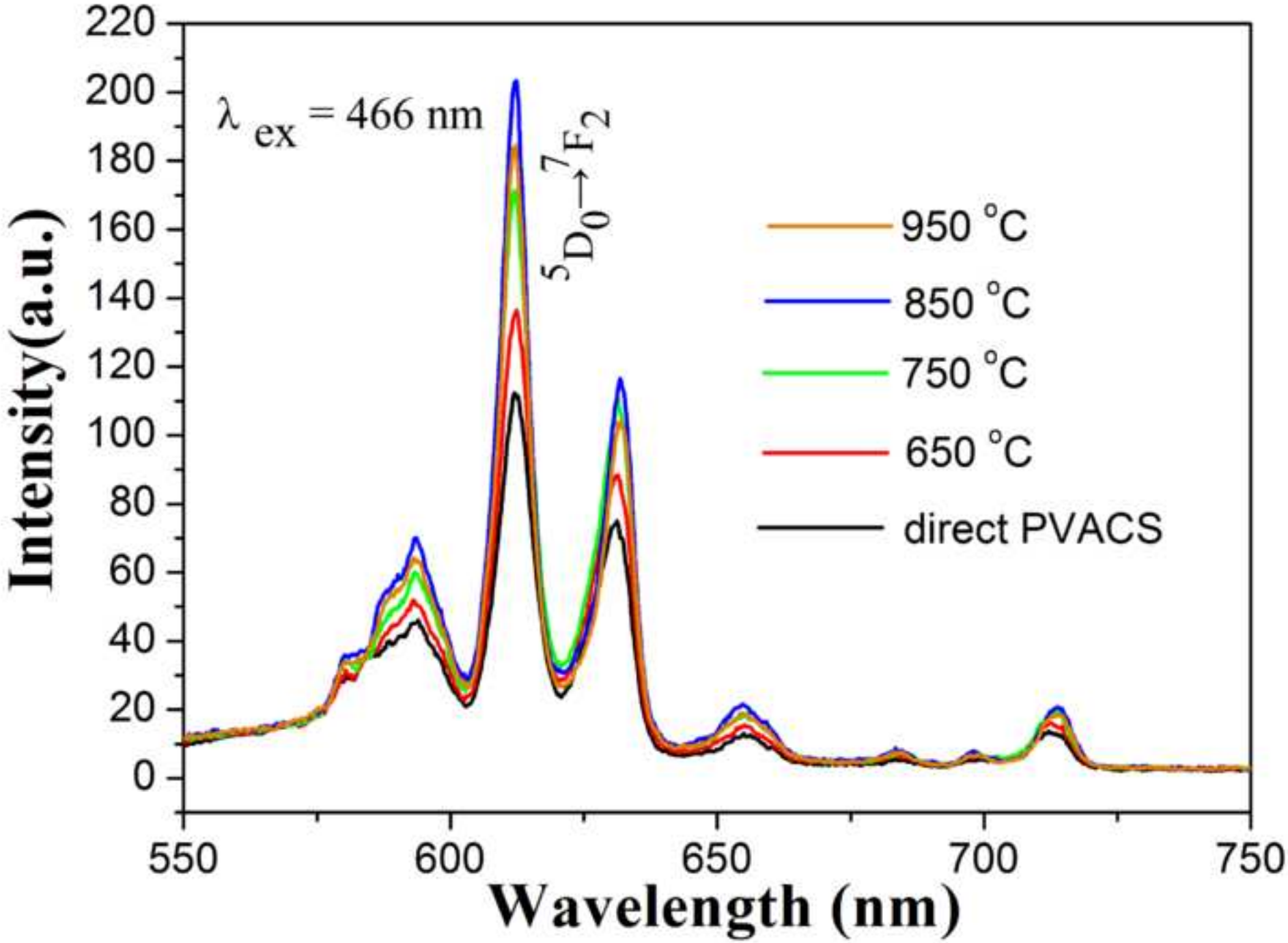

Figure 12

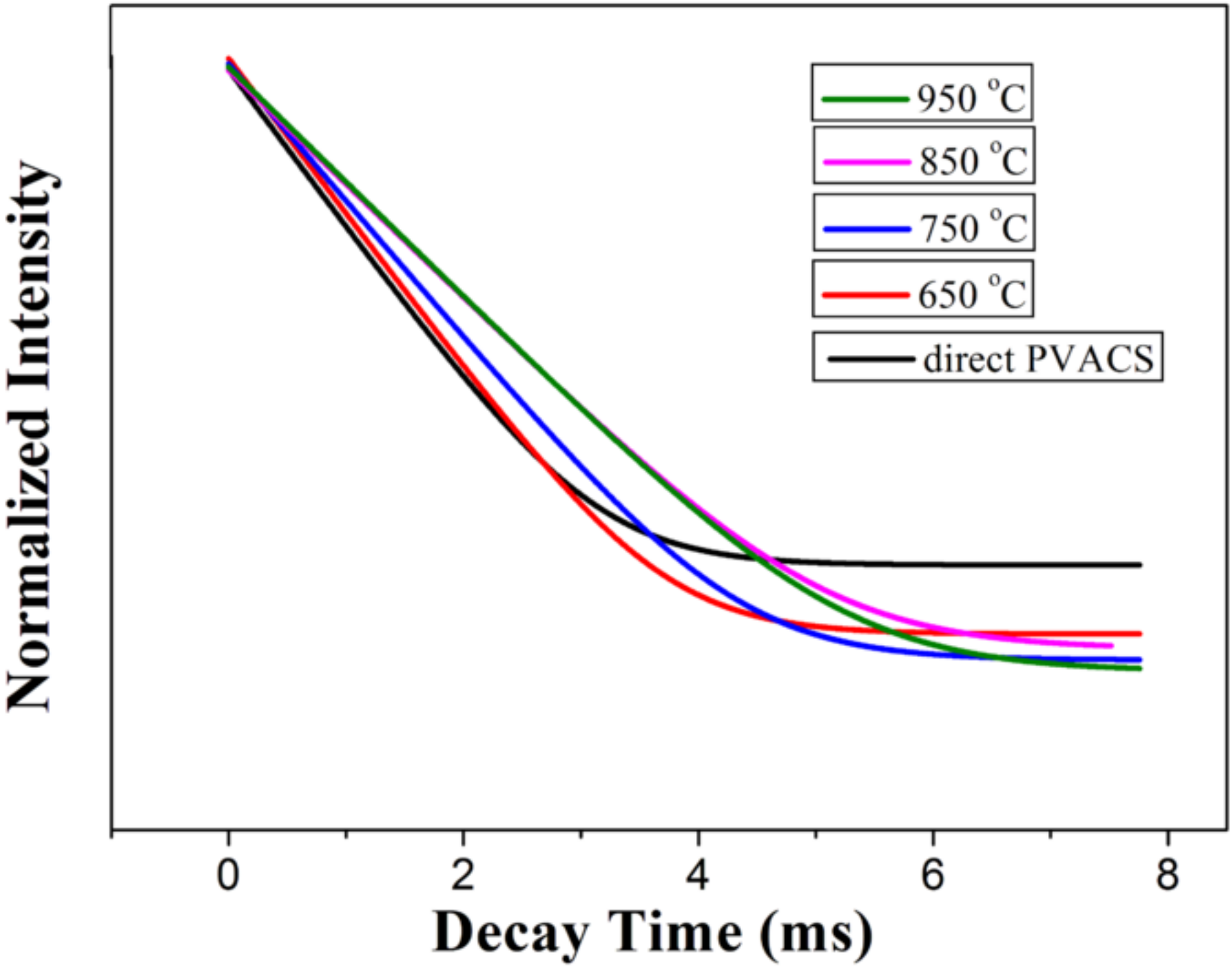

Table 1. The A_{570}/A_{465} and CIE coordinate values of Eu^{3+} -activated $Ce_2LuO_{5.5}$ and CeO_2 samples

Samples	**（A_{570}/A_{460}）**	**CIE coordinate**	
		x	**y**
$Ce_2LuO_{5.5}$	0.4364		
$Ce_{0.86}O_{1.93}$: 0.14Eu		0.570	0.429
$Ce_2Lu_{0.6}O_{5.5}$: 0.4Eu	0.5167	0.583	0.417
$Ce_{1.733}Lu_{0.867}O_{5.37}$: 0.4Eu	0.5989	0.593	0.406
$Ce_{1.6}LuO_{5.3}$: 0.4Eu	0.6324	0.604	0.396

Table 2. The metal elements molar ratio of the Eu –doped $Ce_2LuO_{5.5}$ samples measured by EDS

Composition of Samples	Stoichiometric molar ratio Ce: La: Eu	Measured molar ratio Ce: La: Eu
$Ce_{2-x}LuO_{5.5-x/2}$: xEu (x = 0.1)	1.9: 1.0: 0.1	1.9196: 1.0209: 0.0948
$Ce_{2-x}LuO_{5.5-x/2}$: xEu (x = 0.2)	1.8: 1.0: 0.2	1.8161: 0.9905: 0.2022
$Ce_{2-x}LuO_{5.5-x/2}$: xEu (x = 0.3)	1.7: 1.0: 0.3	1.6492: 1.0634: 0.2819
$Ce_{2-x}LuO_{5.5-x/2}$: xEu (x = 0.4)	1.6: 1.0: 0.4	1.5878: 1.0791: 0.3899
$Ce_{2-x}LuO_{5.5-x/2}$: xEu (x = 0.5)	1.5: 1.0: 0.5	1.4613: 1.0381: 0.4755
$Ce_2Lu_{1-x}O_{5.5}$: xEu (x = 0.1)	2.0: 0.9: 0.1	2.0444: 0.8909: 0.0886
$Ce_2Lu_{1-x}O_{5.5}$: xEu (x = 0.2)	2.0: 0.8: 0.2	2.1045: 0.7748: 0.1874
$Ce_2Lu_{1-x}O_{5.5}$: xEu (x = 0.3)	2.0: 0.7: 0.3	2.1047: 0.6800: 0.2852
$Ce_2Lu_{1-x}O_{5.5}$: xEu (x = 0.4)	2.0: 0.6: 0.4	2.0378: 0.5703: 0.3725
$Ce_2Lu_{1-x}O_{5.5}$: xEu (x = 0.5)	2.0: 0.5: 0.5	2.0635: 0.5172: 0.4607

Table 3. The fluorescent lifetime (τ) and quantum efficiencies (Q) of the composite preparred with PVACS and a subsequent heat-treatment process.

Preparation approach	τ (ms)	Q (%)
Direct PVACS	0.534	12.65
PVACS + 650 ^{o}C	0.549	13.69
PVACS +750 ^{o}C	0.621	15.37
PVACS +850 ^{o}C	0.742	17.92
PVACS +950 ^{o}C	0.734	17.36

Highlights

► $Ce_2LuO_{5.5}:Eu^{3+}$ phosphor nanopowders were prepared by solution combustion reaction.

► Surface morphology and dispersity were evidently improved with surfactant PVA.

► The luminescence of $Ce_2LuO_{5.5}$: Eu^{3+} was greatly enhanced in respect to CeO_2: Eu^{3+}.

► The optimized component was confirmed to be $Ce_{1.6}LuO_{5.3}:0.4Eu^{3+}$.

► Post-sintering process adjusted particle sizes and further promoted luminescence.